# A model for the consolidation of hybrid textiles considering air entrapment, dissolution and diffusion

Werlen, Vincent; Vocke, Richard; Brauner, Christian; Dransfeld, Clemens; Michaud, Véronique; Rytka, Christian

**DOI**
10.1016/j.compositesa.2022.107413

**Publication date**
2023

**Document Version**
Final published version

**Published in**
Composites Part A: Applied Science and Manufacturing

**Citation (APA)**
Werlen, V., Vocke, R., Brauner, C., Dransfeld, C., Michaud, V., & Rytka, C. (2023). A model for the consolidation of hybrid textiles considering air entrapment, dissolution and diffusion. *Composites Part A: Applied Science and Manufacturing*, *166*, Article 107413. https://doi.org/10.1016/j.compositesa.2022.107413

Composites: Part A 166 (2023) 107413

Contents lists available at ScienceDirect

Composites Part A

journal homepage: www.elsevier.com/locate/compositesa

# A model for the consolidation of hybrid textiles considering air entrapment, dissolution and diffusion

Vincent Werlen [a,b,*], Richard Vocke [d], Christian Brauner [a], Clemens Dransfeld [c], Véronique Michaud [b], Christian Rytka [a]

[a] Institute of Polymer Engineering (IKT), University of Applied Sciences and Arts Northwestern Switzerland (FHNW), CH-5210 Windisch, Switzerland
[b] Laboratory for Processing of Advanced Composites (LPAC), Institute of Materials (IMX), École Polytechnique Fédérale de Lausanne (EPFL), CH-1015 Lausanne, Switzerland
[c] Aerospace Manufacturing Technologies, Faculty of Aerospace Engineering, Delft University of Technology, Delft 2629HS, The Netherlands
[d] Faserinstitut Bremen (FIBRE), 28359 Bremen, Germany

ARTICLE INFO

*Keywords:*
B. Permeability C. Analytical modelling E. Consolidation
Resin film infiltration (RFI)

ABSTRACT

A new model is proposed for the consolidation of hybrid textiles, in which air entrapment and dissolution are considered. One of the key parameters is tow permeability, which is described by the analytical model of Gebart and validated at very high fibre volume fractions by direct tow permeability measurement. The model also takes into account the presence of fibres limiting gas diffusion in the molten polymer. Experimental validation of the proposed model is then conducted with quasi-unidirectional glass textile and either polypropylene or polyethylene by measuring the impregnation degree as a function of the consolidation time. Good agreement is found between predictions and measurements for the two matrix systems at different pressures. It is shown that entrapped air significantly influences impregnation. The model offers new and comprehensive insights about the phenomena taking place during consolidation and enables future process optimization.

## 1. Introduction

Fibre-reinforced thermoplastics (FRTP) display several advantages over thermoset-based composites such as a potential for high volume production, better impact resistance and their ability to be recycled [1]. The production of FRTP currently mostly relies on processes using pre-impregnated intermediate materials, for example tapes are employed in automated tape laying and thermoforming is executed with organosheets. Albeit technologically mature, these techniques suffer from the elevated costs of semi-finished products and can only produce parts with limited geometrical complexity [2].

An increasing attention has therefore been given lately to alternative manufacturing techniques as more cost-effective manufacturing techniques for structural parts are sought. Thus, novel techniques such as direct-thermoplastic melt impregnation [3,4], stamp forming of hybrid bicomponent fibres [5] or resin transfer moulding with spacers and high-fluidity thermoplastics [6] have been investigated. Other manufacturing routes generally rely on hybrid systems, meaning that the fibres and thermoplastic are blended at different scales, usually mesoscopically at the ply or microscopically at the tow level. A more intimate hybridization such as in commingled yarns reduces the consolidation time as the matrix flow lengths are reduced [7,8], however the additional mingling step results in higher production costs, especially if a good mingling quality is sought.

In hybrid textiles the polymer and the reinforcing fibres are mingled mesoscopically at the textile level, in hybrid side-by-side textiles for example the reinforcing fibre plies and thermoplastic plies are alternatively stacked as shown in Fig. 1. If flexible thermoplastic plies such as veils are used, the drapeability of the textiles facilitates the production of semi-complex parts. Mingling at the textile level results in lower semi-finished product costs since no microscale homogenization is required but also results in longer impregnation times because of the longer matrix flow length. Nonetheless, Reynolds et al. [9] recently investigated rapid isothermal stamp forming of multilayered textile and thermoplastic veils and proved that this process could produce structural parts within a cycle time of 330 s. Another process suitable for the consolidation of hybrid textiles is two stage press moulding, in which the composite placed into a mould is consolidated in the hot stage of the press before being cooled down under pressure in the cold stage.

* Corresponding author at: Laboratory for Processing of Advanced Composites (LPAC), Institute of Materials (IMX), École Polytechnique Fédérale de Lausanne (EPFL), CH-1015 Lausanne, Switzerland.
*E-mail address:* vincent.werlen@epfl.ch (V. Werlen).

https://doi.org/10.1016/j.compositesa.2022.107413
Received 27 September 2022; Received in revised form 23 December 2022; Accepted 27 December 2022
Available online 30 December 2022

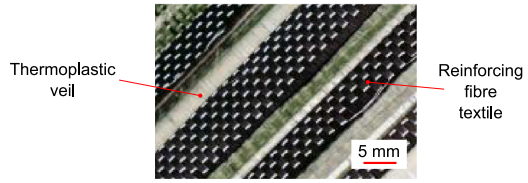


**Fig. 1.** Picture of an hybrid side-by-side textile based on quasi-unidirectional carbon fibres and polyetherimide veils [10]. The textile stack has a partial and staggered cutaway, unveiling the different layers of the stack.

A robust consolidation model is of great importance in these processes for correct parameter setting without trial and error, to correctly estimate void content resulting from incomplete tow impregnation or even for process optimization. Despite a large body of work regarding consolidation, for hybrid textiles no validation over the entire impregnation process has been yet reported. For this reason, preliminary consolidation experiments aiming at measuring the impregnation degree as a function of the time were conducted and large discrepancies between model predictions and experimental measurements were found. Entrapped air was suspected to be responsible for these divergences, requiring development of a new consolidation model taking it into account. Air dissolution and diffusion was deemed necessary to be considered in order to reflect the fact that full impregnation is reached eventually, given enough pressure is applied during consolidation for a sufficient period of time.

In this article, an analytical consolidation model for hybrid textiles is presented. The main novelty lies in the ability of the model to consider air entrapment, dissolution and diffusion. Because voids are almost exclusively located in the unimpregnated region of the tow, void formation and content can also be predicted. Correct prediction of the final void content is relevant in composite production as it is detrimental to mechanical properties [11,12]. The model presented here is restricted to hybrid textiles with woven reinforcement as impregnation of aligned fibre tows is considered as the main mechanism driving consolidation. Existing diffusion models are applied and extended to the diffusion of dissolved species in fibrous reinforcement by adding a correction diffusion factor which is determined experimentally. The model is experimentally validated for film stacking with two different thermoplastics and at different pressures. The model presented in this study is intended for high-performance hybrid textiles and will be validated and extended to those materials in a second stage. In addition, the validity of the model of Gebart [13] for permeability predictions at very high fibre volume fraction is investigated by directly measuring tow permeability with a customized permeability jig. The influence of air entrapment and dissolution on the consolidation kinetics are evaluated, along with other parameters including permeability and effective diffusion coefficient.

### 1.1. State of the art

A large body of work dealing with consolidation in composite manufacturing and its related aspects is found in literature, several of them specifically deal with the impregnation of tows in hybrid textiles. In these models Darcy's law [14] for saturated flow in porous media is systematically used to model matrix flow in fibre bundles. For unsaturated flow, Darcy's law is strictly valid for sharp flow front only, which is also referred to as the slug flow assumption. A micrograph of the flow front in unidirectional carbon fibre tapes presented by Jespersen et al. [15] and in tows presented by Studer et al. [3] for example both suggest validity of this assumption.

Permeability is a key parameter for the description of flow in porous media, yet very difficult to directly measure for tows. Hardly any method to directly measure tow permeability nor related results were presented so far [16,17]. In the literature that parameter is mostly predicted with models, usually with the purely analytical one of Gebart [13] or the semi-analytical Carman–Kozeny model [18]. Even though numerous permeability models and experimental studies were presented [19], the reported tow fibre volume fraction in the literature is often higher than the maximal fibre volume fraction at which transverse permeability was experimentally validated. While tow fibre volume fraction measurements in different studies ranged from 0.58 to 0.78 [20–22] experimental measurements on aligned fibres in the transverse direction were only measured up to 0.59 by Gebart [13] and 0.72 by Gutowski [18]. This means that in consolidation models considering tow impregnation, one of the key descriptors is based on models which have never been validated for the conditions is which they are used.

Early consolidation models considered the reinforcing textile as a layer with homogeneous thickness, for example Phillips et al. [23], Rozant et al. [24] or Jespersen et al. [15] who based their model on the work of Michaud et al. [25–28] and Sommer and Mortensen [29]. Klinkmüller et al. [30] adopted a similar approach for the consolidation of commingled yarns. All these models base their description of consolidation on unidirectional infiltration of molten thermoplastic through the textile layer. Other authors considered the impregnation of an elliptical tow in a bath of molten polymer, such as Grouve et al. [31] and Kobayashi et al. [32] in an approach partially based on the model proposed by Van West [33] for commingled yarn. While some authors assume a constant tow permeability, many model it as a function of the textile compaction stress because permeability depends on the tow fibre volume fraction, which in turns varies with applied stress. Nevertheless, the consensus is that at elevated pressures the change in permeability is rather small [23,32,34] as large pressures are required to obtain small changes in tow fibre volume fractions as documented by Gutowski et al. [18] for aligned graphite fibres.

The different modelling approaches for the impregnation of tows were mostly developed and validated for a specific type of intermediate material architecture such as film stacking or micro-braided textiles. One could argue that consolidation models should in principle be valid for all the different kinds of hybrid textiles since the consolidation kinetics are very similar, the main phenomena always being the impregnation of fibre tows. Yet, no model was validated for different kinds of hybrid textiles. Hence, a direct comparison of the different consolidation models is overall lacking.

Most of the authors assumed that air could freely escape the tow, resulting in atmospheric air pressure in the dry region of the tow. Others, such as Bernet et al. [22] in their model about the consolidation of commingled yarns, introduced a threshold during impregnation after which the air gets entrapped. Rozant et al. [24] considered that air was trapped in the tows during the whole process in their model about the consolidation of knits. The dissolution of air was however not considered and it is interesting to notice that in their experimental validation the void content decreases continuously with longer consolidation times while the model predicts a constant value as shown in Fig. 2.

Entrapped air forms a bubble that can expand or collapse depending on temperature, pressure and species flux at the bubble matrix interface. The dissolution and diffusion of volatiles in liquids has been the subject of a number of studies [35–37] and is commonly described with models based on the Fick's law [38]. The vast majority of research about bubble formation and the related porosity is focused on thermosets because the relatively low applied pressure and the emission of volatiles during curing makes them prone to bubble formation. The models that have been proposed on this topic usually considered the formation of bubble in pure liquids [39,40]. For thermoplastic composites the formation of bubbles in matrix-rich areas is usually disregarded as there is few to no volatile emission during consolidation and the bubbles quickly collapse due to the elevated temperatures and pressures at play.

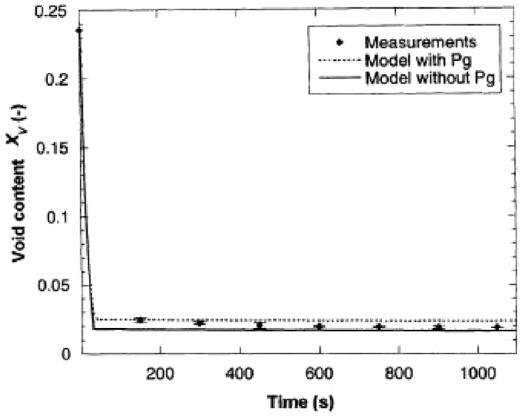


**Fig. 2.** Measured void content as a function of the consolidation time along with model predictions with and without taking into account air pressure $P_g$. One can see that the measured void content continuously decreases while it remains constant in the model predictions. Reproduced with permission from [24].

However, several studies highlighted the difficulty in obtaining full consolidation in fibrous reinforcement due to internal voids [41,42]. Only a few researchers addressed bubble formation and gas diffusion in fibrous reinforcement. Lundström & Gebart [43] modelled void collapse during resin transfer moulding and experimentally determined a geometric correction factor that accounts for the reduced diffusion in bundles since the fibres are almost impermeable. Several studies addressed the diffusion in porous media and proposed correction factor for diffusion, however most focused on gas diffusion and the effect of more complex geometrical effects on diffusion such as fibre tortuosity is not well understood [44–46]. Therefore, for the processing of thermoplastic composites there is an overall a lack of studies and models when it comes to bubble formation and collapse, air dissolution and diffusion, especially in fibrous reinforcements.

## 2. Model approach

### 2.1. Process description

At the beginning of the manufacturing process several plies of hybrid textile are stacked in the mould, each at the desired location and with the desired orientation. At this stage the space between the textile and the polymer film forms air channels at the meso scale. The mould is then placed in a heated press until the process temperature is reached before applying pressure for a given amount of time. In the two-stage press process the mould is subsequently moved to the cold stage while in variotherm press moulding the mould is cooled down. In both processes, cooling down is performed under pressure. Demoulding finally allows yield of the consolidated part.

### 2.2. Initial conditions

During heating up the thermoplastic melts and air starts to diffuse in it, this goes on until the process temperature is reached. Considering the relatively intimate contact between air and thermoplastic and the resulting short flow lengths, it is assumed that the molten thermoplastic has reached the saturation concentration at atmosphere pressure at the beginning of consolidation. As pressure is applied on the mould consolidation begins: as the meso structure collapses the molten thermoplastic will fill the inter-tow space, thereby the air originally located there gets displaced inside the tows as represented in Fig. 3. Therefore, dry tows with an amount $n_\lambda^0$ of entrapped air in moles per unit depth and an inter-tow space filled with molten matrix are considered as initial situation.

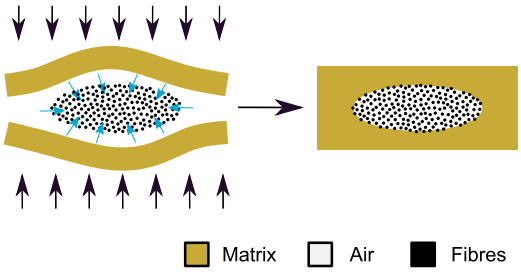


**Fig. 3.** Schematical representation of the initial situation on the left. The meso structure starts collapsing as pressure is applied and air is pushed inside the tows, which results in matrix rapidly filling the inter-tow space as shown on the right. The code colour for the different phases is kept throughout the article.

The amount of air initially present in the textile is approximated to be the same as the amount of air in a stack of pure, uncompacted reinforcing textile. Assuming that the air is equally distributed in the tows, $n_\lambda^0$ reads, as detailed in Appendix A.1:

$$n_\lambda^0 = \frac{P_{atm} \cdot A_{tow} \cdot (1 - v_{f,0}) \cdot v_{f,tow}}{R \cdot T_0 \cdot v_{f,0}} \tag{1}$$

Thereby, $P_{atm}$ is the atmospheric pressure, $A_{tow}$ the cross-section of a tow, $v_{f,0}$ the fibre volume fraction of a reinforcing textile stack at rest, $v_{f,tow}$ the fibre volume fraction inside the tows, $R$ the ideal gas constant and $T_0$ the initial temperature at the time of entrapment. For tows with elliptical shapes with semi major and minor axes $l_w$ and $l_h$ the cross-section area is given as:

$$A_{tow} = \pi \cdot l_h \cdot l_w \tag{2}$$

### 2.3. Impregnation

In the proposed approach it is assumed that the conditions do not vary along the fibre direction. Impregnation of textiles is represented by a two dimensional tow surrounded by a bath of molten thermoplastic as represented in Fig. 3. The underlying assumptions are that the whole surface of the tows is in contact with the matrix, implying that the tow impregnation behaviour is not influenced by neighbouring tows. In addition, there is no gas transport in fibre direction in the unimpregnated region of the tow. Moreover, it implies that the consolidation dynamics in a single average tow are representative of the behaviour at the macro scale. Such an assumption could be violated for example in a textile with large discrepancies in the dimensions of the tow cross-sections as smaller tows will be impregnated faster that the larger ones.

Further assumptions are that the tows have homogeneous fibre volume fraction and permeability, that the matrix pressure in the immediate surrounding of the tow is homogeneous and that the flow front is sharp. Tow dimensions are assumed constant as possible change of tow geometry with applied pressure and its influence on impregnation are neglected. Furthermore, it is assumed that the gas is trapped only in the unimpregnated region of the tow and not in the matrix.

Darcy's law [14] is applied to describe impregnation of the tow, in which the flow front velocity $u$ is related to the tow permeability $K_{tow}$, the tow fibre volume fraction $v_{f,tow}$, the fluid viscosity $\eta$ and the pressure gradient $\nabla P$ as following:

$$(1 - v_{f,tow}) \cdot u = -\frac{K_{tow}}{\eta} \nabla P \tag{3}$$

No analytical solutions to this equation are known for elliptical shapes which tows typically have. Van West et al. [33] proposed to solve impregnation for a cylinder with equivalent hydraulic radius, which was found to have equal fill time. The radius $R_{eq}$ of the equivalent circle is given by:

$$R_{eq} = \sqrt{2} \frac{l_w \cdot l_h}{\sqrt{l_w^2 + l_h^2}} \tag{4}$$

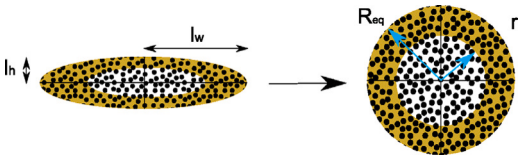


**Fig. 4.** Schematical representation of an elliptical tow cross-section on the left and its equivalent cylindrical shape according to Van West [33] on the right.

A schematic of a partially impregnated tow and its equivalent geometry is shown in Fig. 4, where $r$ is the radial distance to the flow front in the equivalent geometry.

Darcy's law can be resolved for that equivalent circular geometry, as detailed by Bernet et al. [22], thereby mass is conserved:

$$r \cdot ln\left(\frac{r}{R_{eq}}\right)\dot{r} = \frac{K_{tow}}{\eta \cdot (1 - v_{f,tow})}(P_m + P_c - P_g) \tag{5}$$

where $P_m$ is the matrix, $P_g$ the gas and $P_c$ the capillary pressure and the term $(P_m + P_c - P_g)$ will be referred to as the driving pressure. In this article, the capillary pressure is not considered because it is negligible in comparison to the elevated matrix pressures typically occurring during the consolidation of FRTP [22]. The transverse tow permeability $K_{tow}$ is found analytically with the model of Gebart [13], which reads for an hexagonal arrangement:

$$K_{tow} = \frac{16}{9\pi\sqrt{6}}\left(\sqrt{\frac{\pi}{2\sqrt{3}v_{f,tow}}} - 1\right)^{\frac{5}{2}} R_f^2 \tag{6}$$

where $R_f$ is the radius of the fibres. Eq. (5) can be solved numerically as detailed by Bernet and al. [22]. This allows to determine the impregnation degree $\xi$ which is defined as the ratio of the impregnated tow volume over the total tow volume. Considering the equivalent geometry, it therefore reads:

$$\xi = \frac{R_{eq}^2 - r^2}{R_{eq}^2} \tag{7}$$

To find the matrix pressure, mechanical equilibrium is applied and the textile stress response $\sigma_{tex}$ is deducted from the applied pressure $P_{app}$:

$$P_m = P_{app} - \sigma_{tex} \tag{8}$$

A variety of models are available in the literature to describe the stress response of compacted textile stacks [47]. In this article, a quasi-static stress response is adopted because the small strain rates result in little viscoelastic response.

$$\sigma_{tex} = A_{tex} \cdot e^{B_{tex} \cdot v_f} \tag{9}$$

whereas $v_f$ is the fibre volume fraction, $A_{tex}$ and $B_{tex}$ are fitting variables and the function was suggested by Robitaille et Gauvin [48]. More elaborate models taking into account viscoelastic effects could implemented if deemed necessary, for instance the one proposed by Danzi et al. [49].

The fibre volume fraction is a function of the textile areal weight $M_{tex}^A$, the matrix mass $M_m$, the density of the textile $\rho_f$ and matrix $\rho_m$, the number of layer $N$, the tow fibre volume fraction $v_{f,tow}$ and the impregnation degree $\xi$. For an homogeneous plate with cavity area $A_c$ it reads, as detailed in Appendix A.2:

$$v_f = \frac{M_{tex}^A}{M_{tex}^A + \frac{M_m \rho_f}{\rho_m N A_c} + M_{tex}^A \frac{(1 - v_{f,tow})}{v_{f,tow}}(1 - \xi)} \tag{10}$$

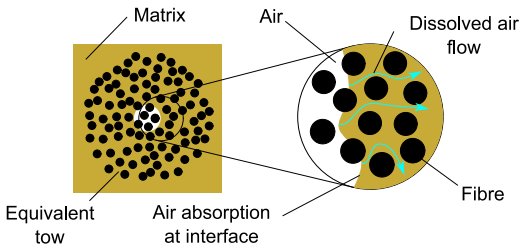


**Fig. 5.** Schematical representation of the diffusion in fibre bundles. Air dissolves at the flow front then diffuses outwards through the interstitial space between the fibres.

### 2.4. Gas diffusion and dissolution

The air pressure is determined with the ideal gas law and depends on the number of moles per unit depth $n_\lambda$, the volume available for the gas to expand $V_g$, the temperature $T$ and the ideal gas constant $R$. In the case of air trapped in a tow, the volume available to the gas depends on the unimpregnated tow volume and its fibre volume fraction. The gas pressure therefore reads:

$$P_g = \frac{n_\lambda \cdot R \cdot T}{V_g} = \frac{n_\lambda \cdot R \cdot T}{A_{tow} \cdot (1 - v_{f,tow}) \cdot (1 - \xi)} \tag{11}$$

where $V_g$ is the volume occupied by the gas per unit depth. As air is absorbed at the interface and diffused into the molten polymer, the amount of air entrapped per unit depth $n_\lambda$ changes over time. Therefore, $n_\lambda$ is obtained based on the initial amount of entrapped air $n_\lambda^0$ by describing its change over time. This implies that the diffusion of air into the polymer has to be described to express the changes of the gas quantity over time. With a flux of species $J$ per unit depth the temporal change of entrapped gas reads, considering that in the equivalent geometry the surface available for diffusion is the surface of the cylinder with radius $r$:

$$\dot{n}_\lambda = 2 \cdot \pi \cdot r \cdot J \tag{12}$$

The approximate solution for the diffusion of gas bubbles in liquids proposed by Epstein and Plesset [40] is applied to determine the flux of species. As fibres are assumed impermeable, the dissolved species can only diffuse in the interstitial space between the fibres as represented in Fig. 5 and diffusion will thus be lower than in pure polymer. Therefore, the diffusion in fibre bundles is described with the diffusion coefficient in pure polymer $D$ corrected with a correction factor $G$. Inserting the Equation of Epstein and Plesset into the previous one yields:

$$\dot{n}_\lambda = -2 \cdot \pi \cdot r \cdot G \cdot D \cdot (C_s - C_\infty) \cdot \left(1 + \frac{1}{\sqrt{\pi DGt}}\right) \tag{13}$$

where $C_s$ is the saturation concentration at the bubble interface and $C_\infty$ the far-field concentration, which is assumed to be the saturation concentration at atmospheric pressure as mentioned earlier. The saturated concentration of a species in a medium is dependent on the pressure $P$ following Henry's law:

$$C_s = H_c \cdot P \tag{14}$$

where $H_c$ is Henry's constant, which is specific to each gas/medium system. In this article, the air is simplified as pure nitrogen which makes up the large majority of air composition. However, it is possible to consider an air mix, which would require to calculate the diffusion of each gas separately.

## 3. Materials and material characterization

Glass fibres woven fabric with a quasi-unidirectional (UD) Leno weave fabric architecture, a silane sizing and an areal weight of 931 $\frac{g}{m^2}$ provided by Tissa Glasweberei AG was used in this study. This

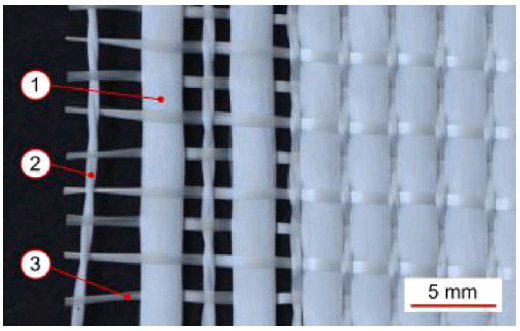


**Fig. 6.** Close-up picture of the fabric. The main tow is indicated by (1) and the supporting weave by (2) and (3).

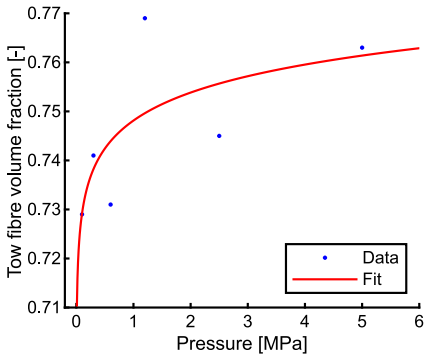


**Fig. 7.** Measured and fitted tow fibre volume fraction as a function of pressure.

fabric consists of main tows free of crimps held together by smaller tows in both the weave and weft direction that will be referred to as the supporting weave. Fig. 6 displays a close-up picture of the weave where the main tows and the supporting weave can be distinguished. The main tows in the weave direction have 2400 tex with and a density of 3.5 $\frac{\text{tows}}{\text{cm}}$. The supporting weave consists of two twisted tows with each 68 tex with a density of 3.5 $\frac{\text{tows}}{\text{cm}}$ in the weave direction and 68 tex tows with a density of 5 $\frac{\text{tows}}{\text{cm}}$ in the weft direction.

The density of the fabric $\rho_f$ was measured to be 2524 $\frac{\text{kg}}{\text{m}^3}$ with the buoyancy method using a precision scale with an immersion set-up and three samples. Micrograph analysis of textile cross-section indicated that the main tow geometry could be well described with an ellipse with semi-major and minor axes $l_w$ and $l_h$ measured to be 1.1 and 0.33 mm. Composite plates were manufactured by wetting textile plies with thermoset resin and curing them under pressure while letting excess resin flow out to ensure load transfer to the textile. Micrographs were produced with plates pressed at different consolidation pressures. Then, a MATLAB® script was used to detect the fibres with a circular hough transform based method and measure the tow fibre volume content and fibre diameter. The tow fibre volume fraction as a function of the applied pressure was fitted to a function of the form $A_{tow} \cdot log(P_{app}) + B_{tow}$ based on Eq. (9) by least square fitting of the error between the curve and the fit. The measured tow fibre volume fraction as a function of the pressure is shown in Fig. 7 along with the fit, thereby one repeat was done at each different pressure. The coefficient $A_{tow}$ was measured at $8.23 \cdot 10^{-3}$ and $B_{tow}$ at 0.6344. The dependence of the tow fibre volume fraction on the applied pressure is weak, in line with previous research. The packing of the fibres can be overall well described with a hexagonal arrangement and the fibre diameter was measured to be 9.0 μm.

Two thermoplastics were investigated in this study, polypropylene (PP) BJ100HP from Borealis and high density polypropylene (HDPE) Lupolen 5236 HX from LyondellBasell. The technical datasheets specify that the PP has a melting temperature of 165 °C and a density of 906 $\frac{\text{kg}}{\text{m}^3}$ in solid state while these values are respectively 133 °C and 952 $\frac{\text{kg}}{\text{m}^3}$ for the HDPE. The polymers were obtained in the form of granulates and were transformed in 0.15 mm thick foils with a Collin extruder.

The zero-shear viscosity $\eta_0$ of the molten polymers were measured at 0.1 $\frac{1}{\text{s}}$ with an Anton Paar Physica MCR 300 plate–plate rheometer at 190 °C. The viscosities of PP and HDPE were found to be respectively 495 and 5440 Pa s. The densities of the molten polymers were measured to be respectively 763 and 786 $\frac{\text{kg}}{\text{m}^3}$ for PP and HDPE at 190 and 160 °C with a MI-2 melt flow indexer. The solubility and diffusion coefficients were taken from the work of Sato et al. [50] at a temperature of 190 and 160 °C for respectively PP and HDPE. Henry's constants $H$ for the dissolution of nitrogen ($N_2$) in polypropylene and high-density polyethylene melt of $3.6 \cdot 10^{-5}$ $\frac{\text{mol}}{\text{Pa m}^3}$ for PP and $4.3 \cdot 10^{-5}$ $\frac{\text{mol}}{\text{Pa m}^3}$ for HDPE were used. The nitrogen diffusion coefficients $D$ of $5.0 \cdot 10^{-9}$ $\frac{\text{m}^2}{\text{s}}$ for PP at 190 °C and to $6.0 \cdot 10^{-9}$ $\frac{\text{m}^2}{\text{s}}$ for HDPE at 160 °C were used. Thereby, the influence of the weight fraction of dissolved gas in the polymer described by Sato et al. [50] for very high pressures was neglected.

The reinforcing textile stress response was measured with a Zwick Roell Z100 universal testing machine equipped with 135 mm perforated steel plates in [47]. The plies were individually coated with the silicone oil Xiameter PMX 200 (Dow Europe GmbH), to obtain a similar lubricating effect as the molten polymer. The fibre volume content at rest $v_{f,0}$ was measured to be 0.414 and a value of 0.03 and 24.2 for the parameters $A_{tex}$ and $B_{tex}$ were found.

### 3.1. Tow permeability

Due to the lack of experimental validation at such elevated fibre volume fraction, it was decided to directly measure the tow permeability in order to check the value predicted by the analytical model. The experiment was performed with a through-thickness permeability jig that is schematically represented in Fig. 8 and was described in detail in other studies [3]. The jig was originally meant for circular samples, which are placed in the cavity between two aluminium honeycombs applying pressure on it. To measure permeability, pressurized oil is let at the one end of the jig and freely flows out at the other end in a recipient that is continuously weighed.

Because manufacturing a circular sample and placing it in the jig without disturbing the loose fibres would be difficult, an adapter was placed inside the cavity to measure permeability on square samples instead. The adapter is a 10 mm thick circular polymethylmethacrylate (PMMA) in the middle of which is a square hole with a side of 50 mm, as shown in Fig. 9(a), where the sample is placed. A sealing on the outside prevents oil from flowing in the interstitial space between the adapter and the jig, which would perturb the measurements. On the top and bottom of the sample are placed 2 mm thick laser cut PMMA meshes with minimal flow resistance. The adapter is meant for samples with a thickness between 6 and 10 mm so that the pressure is transferred on the sample and not to the adapter itself. Fig. 8 schematically represent the jig as described by Studer [3] on the left and as modified with the adapter placed inside on the right.

To directly measure the tow permeability a UD fibre stack was created with the tows. Because the rowing spool with which the weave was manufactured was not available, the tows were directly extracted from the fabric. This was done by cutting single plies to rectangles with a length of 50.1 mm in the weave direction with a CNC cutting machine and manually withdrawing the tows as shown in Fig. 9(b). The tows were cut slightly longer than the cavity width to avoid gaps between the sample and the adapter cavity which could disturb the permeability measurement. The amount of tows placed in the cavity was defined such as to obtain a layer with a thickness $h_{PT}$ that was set to 7 mm. A layer with constant thickness, density $\rho_f$ and fibre volume fraction $v_{f,tow}$ in the cavity with area $A_C$ will have a mass $M_{PT}$ given by:

$$M_{PT} = \rho_f \cdot A_C \cdot h_{PT} \cdot v_{f,tow} \tag{15}$$

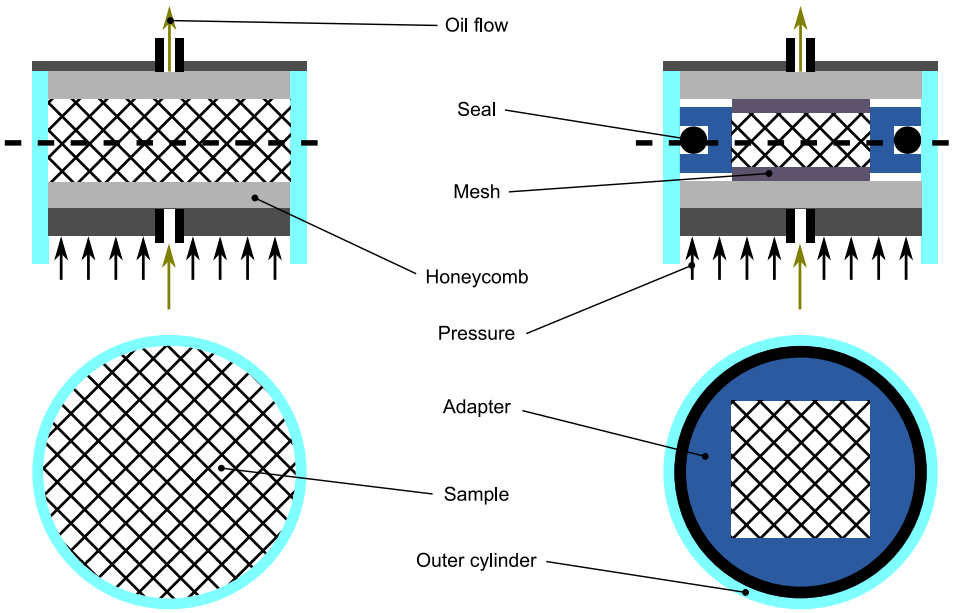


**Fig. 8.** Schematic representation of the jig used in this study, as presented by Studer et al. [3] on the left and as modified in this study on the right. The upper half shows a vertical cut of the jig while the bottom half represents a top cut view, whereas the cut is at the level of the dashed line.

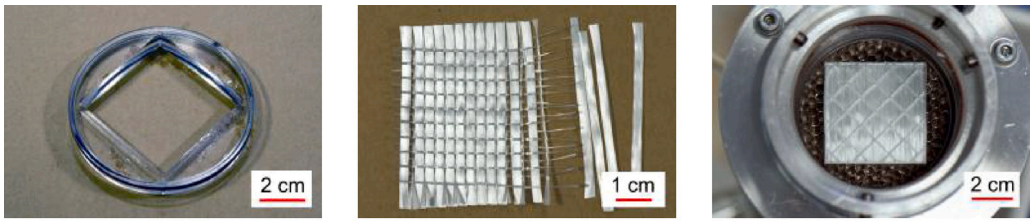


**Fig. 9.** Representation of the process for preparing a UD samples. A picture of the adapter is shown in Fig. 9(a), where the square hole for the sample and the seal can be seen. The tows are extracted from the textile cut with a CNC cutting machine as shown in Fig. 9(b). The adapter with the sample is finally placed in the permeability jig as shown in Fig. 9(c). The adapter itself is transparent and cannot be distinguished in the picture, instead the aluminium honeycomb underneath appears. In the middle of the adapter the sample can be seen with the PMMA mesh placed on top of it.

The tows were extracted until the target weight $M_{PT}$ was reached before being carefully and evenly placed in the cavity in an aligned fashion as shown in Fig. 9(c). The pressure applied on the sample soaked in silicon oil was then gradually raised before letting it rest for an hour in order to give time to the tows to rearrange themselves and close possible gaps. The permeability measurement was performed with the silicone oil Xiameter PMX 200 (Dow Europe GmbH) with a viscosity of 0.1 Pa s, a pressure on the fibres of 1 MPa and an oil pressure of 0.15 MPa. The experiments was performed three times, each time with a virgin sample. Fig. 8 schematically represents how the jig used in this study was modified to allow direct tow permeability measurement.

The tow permeability was measured to be $4.3 \cdot 10^{-14}$ Pa s with a standard deviation of $1.8 \cdot 10^{-14}$ Pa s. For comparison, the predicted permeability for a pressure of 1 MPa reads $6.1 \cdot 10^{-14}$ Pa s. Fig. 10 display the predicted permeability as a function of the applied pressure along with the measured permeability. The permeability was predicted according to Eq. (6) and the tow fibre volume fraction which depends on the applied pressure as shown in Fig. 7.

Given the model predictions typically spanning several orders of magnitude depending on the fibre volume fraction and considering the usually reported accuracies of the different models [19], the difference between measured and predicted permeability is well within acceptable bounds. The relatively elevated standard deviation reflects the difficulty to measure materials with such low permeabilities, as tiny gaps or small non uniformity in sample thickness can significantly affect the result. Nonetheless, this result indicates that the analytical model of Gebart can be reasonably applied to predict tow permeability at very elevated fibre volume fractions.

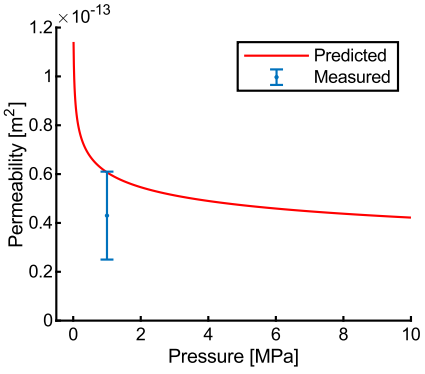


**Fig. 10.** Predicted tow permeability as a function of the applied pressure for the textile investigated in this study, along with the measured permeability.

## 4. Methods

The experiment consisted of consolidating plates for different periods of time and subsequently measuring their impregnation degree.

**Table 1**
Overview of the experiments including process parameters.

| Thermoplastic | Textile | Number of layers | Press temperature [°C] | Process temperature [°C] | Pressure [MPa] | Press time [min.] |
|---|---|---|---|---|---|---|
| PP | Glass quasi-UD | 5 | 200 | 190 | 1.04/1.73/3.46 | 0/2/5/15/30/60 |
| HDPE | Glass quasi-UD | 5 | 170 | 160 | 1.73/3.46/6.92 | 0/2/5/15/30/60 |

This allowed to measure the impregnation degree over consolidation time and compare it against model predictions, whereas the diffusion reduction factor $G$ was fitted to the measurements. In order to validate the impregnation model, the experiment was then repeated at different pressures and with different materials as summarized in Table 1.

### 4.1. Experimental test setup

For the experiments, film stacking was chosen and each textile layer was placed between two 0.15 mm thick thermoplastic foils, such as to target a final fibre volume fraction of 0.55. The textile plies were cut to the dimensions of the mould with a CNC cutting machine while the thermoplastic foils were cut by hand with a cutter and a stencil, in total 5 plies of textile and 10 of foils were required for each plate. While the weight of the textile was calculated based on the areal weight and the area the thermoplastic foils were weighed prior to consolidation.

The plies were then placed into a custom 170 × 85 mm plate mould, thereby great care was taken to disturb the textile architecture as little as possible. A two-stage 200 kN Vogt hydraulic press was used for the experiments, whereas one stage was heated and the other one water cooled. At the beginning of the experiment the mould containing the plies was placed in the heated press, which temperature was set to 200 °C for polypropylene and 170 °C for polyethylene. Pressure was already applied during heating up to ensure contact with both the top and bottom part of the mould and reduce temperature inhomogeneities, thereby a spacer was inserted to prevent the pressure from translating to the composite.

The mould was let up to heat whilst monitoring the cavity temperature with a thermocouple until five degrees below the process temperature specified in Table 1, at which point the spacers were removed and pressure applied to start consolidation. Thermal monitoring revealed that the cavity temperature did not exceed 5 °C above the specified process temperature. These slight thermal variation were neglected and the cavity temperature was assumed constant at the specified process temperature in Table 1. This implies that other temperature dependent material properties such as viscosity and diffusion coefficient were assumed constant as well. After the given press time was elapsed, the mould was transferred to the cold stage and cooled down under pressure. The transfer lasted up to 30 s, during which no pressure was applied onto the mould.

Early heating up trials with several thermal sensors indicated an homogeneous temperature throughout the mould when the consolidation starts. The time required for the mould to reach the melt temperature during the cooling down was measured not to exceed 2 min. Since impregnation goes on during cooling down as pressure is applied, the total consolidation time was conservatively defined as the press time plus 1 min. +/− 1 min.

### 4.2. Analysis

The consolidated plates were cut transverse to the fibre directions with a Compcut 200 composite circular saw. Microscope analysis of polished samples was found to be difficult because of the tendency of debris material to fill up the voids, which were then hardly distinguishable from matrix. Therefore, the cut surface was then directly photographed in high resolution with a Nikon D810 equipped with a AF-S VR Micro-Nikkor 105 mm 1:2,8G IF-ED objective. The impregnation degree was measured with the software ImageJ by manually selecting and measuring the dry and the whole area of at least 30 tows per sample. The semi-minor and major axes of the tows were also measured with an integrated plug-in of ImageJ automatically fitting ellipses over the selected area. The outer textile layers were not included in the measurements because the cutting process slightly deconsolidated them and the tows close to the sides neither to avoid potential edge effects.

The diffusion reduction factor $G$ was obtained by minimizing the sum of squares differences between the model predictions and the measured impregnation degrees with an interval halving algorithm based script in MATLAB®.

## 5. Results

Plates could be successfully produced without deviation from the test plan and mould remained sealed during the trials as only negligible amounts of polymer flowed in the shear edge clearance. The plates did not show any visible defect and had a final thickness of about 3.8 mm with some slight variation depending on the impregnation degree. A picture of a plate cross-section is shown in Fig. 11(a), which presents homogeneous properties in terms of thickness, tow spacing and impregnation degree. A close-up is displayed in Fig. 11(b), where one can distinguish between the dry and impregnated regions of the tow. A narrow gap is present between the tows in all directions, meaning that the assumption of a tow in a bath of molten thermoplastic as represented in Fig. 3 on the right is well founded. In addition, no bubbles were observed in the inter-tow region and similar observations can be made in pictures presented in other studies [15,31], which confirms the assumption that the gas is trapped only in the unimpregnated region of the tow.

The tow dimensions within each plate were found to be rather constant as the standard deviation of the semi-minor and major axis was measured between 3 and 4%, whereas a significant portion of this value might be induced to measurement inaccuracies since measurements were performed by hand. When comparing the average values of the different plates, variations in the order of 5% are found. The correlation between tow dimensions and pressure or impregnation degree, which is linked to the degree of compaction, is almost non-existent.

Fig. 12 shows the results of the whole set of consolidation experiments. At the very beginning the impregnation degree quickly raises, then a plateau value is reached and impregnation progresses much slower. The impregnation model fits the experimental measurements quite well and is able to explain the observed behaviour for different pressures and materials. At first, impregnation is dominated by matrix flow in the tow, then air pressure builds up and opposes further impregnation, which results in a plateau. At this point, air dissolution and diffusion is necessary for further impregnation and the rate at which this takes place determines the slope of the plateau. In the following, the first stage of impregnation will be referred to as the *pressure difference driven impregnation* while the second stage will be referred to as the *dissolution driven impregnation*. Overall, the model can capture all relevant phenomena and predict consolidation reliably, both during the matrix flow and the diffusion dominated parts.

Fig. 12(a) shows an increasing mismatch between predictions and measurements at the beginning of consolidation with increasing pressure. This is attributed to deconsolidation taking place during displacement of the mould to the cold stage, during which no pressure is applied. The matrix pressure vanishes thereby, yet the air trapped in the tow is still pressurized and therefore drives the matrix out. In Fig. 12

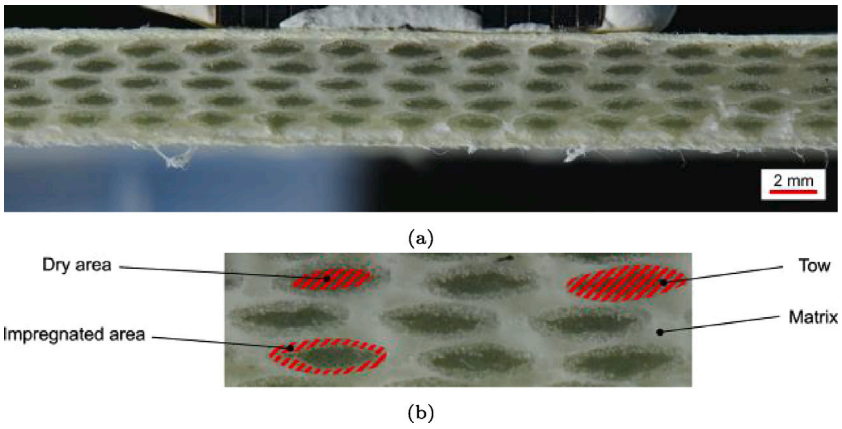


**Fig. 11.** 11(a): Picture of a cross section of the plate with PP matrix consolidated at 1.04 MPa for 5 min. 11(b): Close up of picture 11(a), where the dry and impregnated zones of the tows can be distinguished.

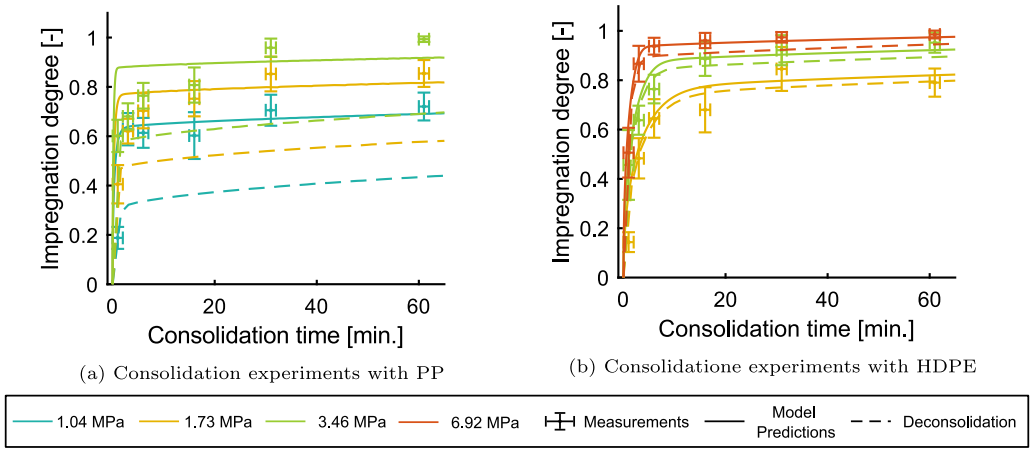


**Fig. 12.** Measured and predicted impregnation degree as a function of the consolidation time for PP in Fig. 12(a) and HDPE in Fig. 12(b) with different consolidation pressures, along with minimal predicted impregnation degree resulting from deconsolidation during mould transfer from the hot to the cold stage.

the dashed line is obtained by adding, at the end of the given consolidation time, 30 s without matrix pressure at the end to reflect the deconsolidation taking place during displacement of the mould to the cold stage. One can see that while for experiments with HDPE the effect of deconsolidation is limited, for PP however it becomes relevant. This is linked to the higher viscosity of HDPE, which results in slower matrix flow and de-consolidation kinetics in a similar fashion as reported by Wolfrath et al. [51]. One should stress that this calculation represents an absolute conservative estimation of the conservation, because during cooling pressure is applied and the composite at least partially reconsolidates. Nonetheless, this strongly indicates that the observed deviation between predictions and measurements can be imputed to experimental error caused by deconsolidation when transferring the mould from the hot stage to the cold stage.

The diffusion reduction factor $G$ was fitted to a value of 2.3 e-4, thereby the experiments with PP were omitted because of the perturbation caused by deconsolidation and the same value of $G$ was used for all experiments. The diffusion reduction factor is a purely geometrical effect and is certainly directly influenced by the fibre packing, in this study the change of tow fibre volume fraction with applied pressure is only minimal as reported in Fig. 7 and was neglected. The low value obtained for the diffusion reduction factor indicates a very strong reduction of diffusion by the highly packed fibres. From the experiments with PP it seems that air diffusion is slightly underpredicted, which is attributed to an imprecise diffusion coefficient definition of the polymers since literature values were employed.

Fig. 13 shows the measured impregnation degree of the plate with polypropylene consolidated at 1.04 MPa along with the predictions of the consolidation model. In addition, two further predictions are presented: one where it is assumed that only the air originally present in the tows gets entrapped without diffusion and one where air entrapment is neglected.

Assuming that only the tow originally present in the air gets entrapped results in a plateau value significantly higher than the measured values, even when assuming no diffusion at all, which strongly hints at a higher amount of entrapped air. If air entrapment is neglected, the proposed model becomes similar to those proposed in the literature so far. Neglecting air entrapment yields, at the beginning, impregnation curves which are very similar to the model proposed in this article. However, the plateau value is not captured. There is a large difference between the different models in terms of time predicted for complete impregnation. This could explain the observations of Grouve et al. [31], who noted a large discrepancy between the time predicted by models available in the literature for complete impregnation and the press times used in practice.

The textile stress response as modelled through Eq. (9) was found to be surprisingly negligible and to take up less than one percent of the applied pressure, even for the lowest consolidation pressure of 1.04 MPa. The fibre volume fraction at the meso scale depends on the impregnation degree as expressed through Eq. (10), which implies that the textile stress response changes during consolidation. Fig. 14 shows the fibre volume fraction and the textile stress response at different

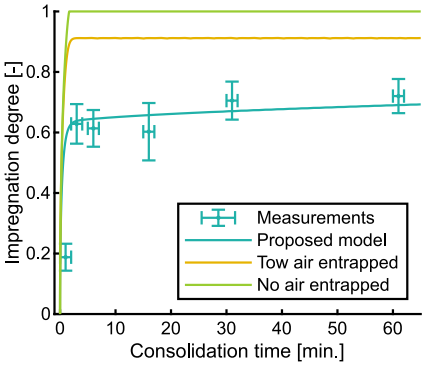


**Fig. 13.** Measured impregnation degree as a function of the consolidation time for PP and a pressure of 1.04 MPa, along with the model prediction and the model predictions assuming only tow air entrapped and no air entrapment.

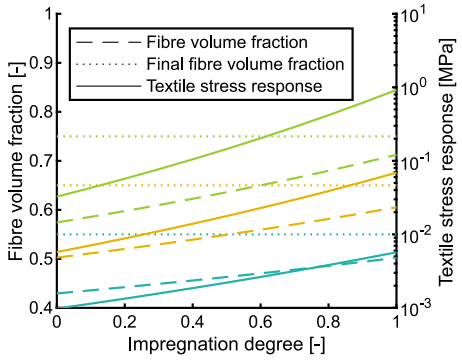


**Fig. 14.** Fibre volume fraction and textile stress response as a function of the impregnation degree for a tow fibre volume fraction of 0.75, HDPE matrix and different targeted final volume fractions of 0.55, 0.65 and 0.75.

final volume fractions depending on the impregnation degree. This result was obtained with HDPE and a tow fibre volume fraction of 0.75 resulting from an applied pressure of 1 MPa. One can see that very elevated final volume fraction have to be targeted for the portion of applied pressure taken up by the textile to become significant.

Fig. 15 schematically shows how the compaction state changes during consolidation and helps to understand the results displayed in Fig. 14. As impregnation goes on matrix will fill in porosities and reduce the volume taken by the composite. Since the amount of textile is confined in a smaller volume, the plies are automatically more compacted and the textile stress response increases. When the composite is cooled down the matrix solidifies and shrinks, which once again cause a reduction of the whole composite volume and thus a higher fibre volume content. This also explains why in Fig. 14 the fibre volume fraction at full impregnation differs from the final fibre volume fraction in solidified state. These phenomena can also be read from Eq. (10), where both the impregnation degree and the matrix density influences the fibre volume fraction and thus textile stress response following Eq. (9). Now, the densities of the solid and molten matrix differ quite significantly and this explains why plates with elevated final volume fractions in solid state will still have moderate fibre volume fractions and textile stress response during processing in molten state.

## 6. Discussion

Two stages can be differentiated during the impregnation of hybrid textiles, one pressure difference driven matrix flow and driven by air dissolution and diffusion. Several assumptions and simplifications are met for the pressure difference driven matrix flow, such as assuming that the whole surface of the tow is in contact with molten polymer, which was found here to be valid. Other simplifications, such as neglecting the change of viscosity with shear rate are commonly met in the literature. Some of these assumptions were addressed and justified, other are thought to have a limited effect on consolidation.

The tow permeability $K_{tow}$ and the diffusion reduction factor $G$ are two major sources of uncertainty, both being difficult to predict accurately. Figs. 16 and 17 show respectively the influence on the permeability $K_{tow}$ and the diffusion factor $G$ on impregnation with an applied pressure of 1.73 MPa and HDPE matrix. In both cases, the gold line represents the proposed model predictions, the blue line the model prediction with lower variable value and the green line the model prediction with higher variable value. One can see that the tow permeability influences to some extent the pressure difference driven flow and the time at which the transition to the diffusion driven flow takes place. Afterwards however, the different lines can hardly be differentiated from one another. It is not surprising for the diffusion driven flow to be barely influenced by permeability, as it only influences the rate at which pressure equilibrium between matrix and air is achieved but has no direct influences on diffusion itself once that equilibrium is achieved. Therefore, the uncertainty and error bound with the permeability determination has a limited influence on the overall consolidation behaviour and almost negligible for the consolidation time required for complete impregnation. Regarding the diffusion factor, one can see that the diffusion reduction factor barely affects the pressure difference driven impregnation but influences the dissolution driven impregnation. A higher diffusion reduction factor, which results in a higher effective diffusion coefficient, increases the rate at which dissolution takes place and increases the slope of the impregnation degree curve during the dissolution driven impregnation.

This study presents a methodology to directly measure tow permeability at the highest fibre volume fraction reported, to our best knowledge, so far. The results indicate weak dependence of the tow fibre volume fraction on the applied pressure, however other types of tows such as recycled carbon fibre bundles there might be more compressible and more accurate methods to determine tow fibre volume fractions might be desirable. The results also indicate that the permeability model according to Gebart [13] at very elevated fibre volume fractions is reasonably accurate. It would yet be of interest to enhance the test setup to increase measurement accuracy and decrease scatter in future studies. Considering that tool compliance was found to be a major source of error in permeability measurement [52], it would make sense to use stiffer materials such as steel in the permeability measurement device. Furthermore, building the device in such a way that it can be placed in a universal testing machine during testing would allow to accurately determine at the same time the relation between applied pressure, fibre volume fraction and permeability.

The air dissolution and diffusion models fit the experimental data well for different polymers and in different conditions, yet some questions marks remains. For instance, the air dissolution and diffusion coefficients in pure polymer should be experimentally measured using for example the equipment described by Sato et al. [53] as for many of them no values were found in the literature nor is the required testing equipment commonplace. It is desirable to have a purely predictive model, meaning that in future work models should be developed to predict the diffusion reduction factor in fibre bundles. This factor is most probably influenced by the fibre volume fraction as fibres obstruct diffusion, the tow microstructure could also play a role. For instance the tortuosity of the open pores could make the diffusion path longer and hinder diffusion. Investigation of the microstructure as presented for instance by Gomarasca et al. [54] might prove necessary to fully understand the mechanisms at work.

Since the importance of air diffusion has been proven to play a major role in this study, the ability of polymers to dissolve air could become a major selection criterion in the production of hybrid textiles

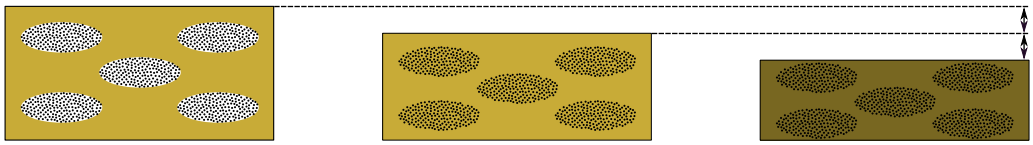

**Fig. 15.** Schematical representation of how the compaction state changes during consolidation. The initial state is shown in the left, the fully impregnated state in the middle and the final state after cooling on the right. The light beige shade indicate molten polymer while the darker shade indicates a solidification.

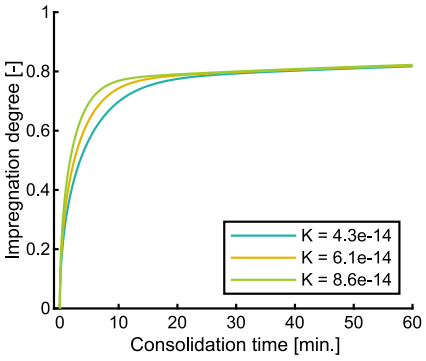


**Fig. 16.** Influence of the tow permeability $K_{tow}$ on the impregnation behaviour according to the proposed model for a pressure of 1.73 MPa and HDPE as matrix.

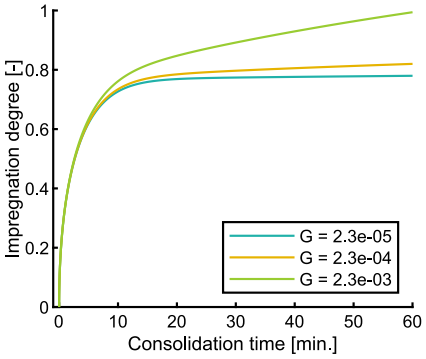


**Fig. 17.** Influence of the diffusion reduction factor $G$ on the impregnation behaviour according to the proposed model for a pressure of 1.73 MPa and HDPE as matrix.

based thermoplastic composites. Instead of focusing heavily on the development of very low viscosity thermoplastics such as the PP used in this study or the polyamide 6 "Evolite HF XS1480" from Solvay [3,4], their ability to absorb and diffuse air should also be weighed. In addition, the possibility to use existing additives or develop new ones should be considered. Furthermore, as the solubility of gases with low critical temperatures such as nitrogen decrease with increasing temperature [50], this should also be considered when selecting process parameters.

The model presented here assumes that the dimensions of the tow are constant, which was in agreement with experimental observations. Other studies such as the one presented by Kobayashi et al. [32] reported more significant tow flattening during consolidation, but also found that denser fabrics and the presence of several plies inhibited tow flattening. Future studies should quantify both the tow deformation and the influence it has on the accuracy of the consolidation model. The little tow deformation observed in this study is not only attributed to the large tow size, but also to the sizing and the Leno weave architecture that is particularly stable.

The final fibre volume fraction of 0.55 targeted in this study is already quite elevated, yet the assumption of a tow in a molten polymer bath assumption was found to remain valid. The textile stress response was found to amount for less than 1% of the applied stress, even for consolidation at 1.04 MPa, the lowest applied pressure in this study. In future research, one should investigate if the model remains accurate for other textiles and at higher fibre volume fractions. When compared to film stacking which was used in this article for experimental validation, hybrid textiles based on veils for example could have additional air trapped in the polymer layer because of its structure, which is why experimental validation with other architecture of hybrid textile is desirable. At higher fibre volume fractions, the impact of the whole tow surface no longer being in contact with molten polymer, if occurring, should be assessed. As a result of the increasing polymer density during solidification, the fibre volume fraction and thus textile stress response can rise sharply during cooling down, thereby resulting in a decreasing matrix pressure. An insufficient matrix pressure in injection moulding is known to favour void formation as a result of polymer shrinkage [55], in addition lower matrix pressure could potentially result in higher void content as entrapped air bubbles in the matrix will expand or because of the nucleation of absorbed volatiles [39]. Hence, textile stress response during solidification should not be overlooked during composite production.

The experimental results with PP highlight the sensitivity of two-stage press moulding to deconsolidation. If the process allows for a very fast impregnation, then an equally fast deconsolidation is to be expected and even short deconsolidation times can have very significant effects. Rapid isothermal press moulding where heating and cooling is integrated in the mould seems a preferable option for the consolidation textiles as it removes the risk of deconsolidation altogether. If two stage press moulding is used, swift displacement from to the cold stage is necessary. Alternatively, cooling upon full consolidation is also possible as the whole air is dissolved and cannot drive the matrix out.

The model presented here allows for a comprehensive understanding of the different phenomena taking place during consolidation, and sheds light on new mechanisms. Even though the influence of each parameter can be assessed, it is still unclear at this point what the optimal set of process parameters is. A set of investigations will be conducted in future work to understand if higher pressures result in a faster dissolution of the air in the molten polymer and how does the total impregnation time scales with different parameters such as tow size or temperature. In any cases, applying elevated pressure remain a possible consolidation strategy to reduce void size if not completely eliminating it, yet too elevated pressures can cause fibre damage. Another parameter which should be investigated is the temperature, as increasing it decreases the viscosity and the solubility of nitrogen in polymers (those investigated so far). Therefore, higher temperatures do not necessarily result in faster impregnation times. A strategy could be to variate the temperature such as to have low viscosity during the pressure driven flow and then decrease the temperature to enhance dissolution.

The results presented in this study shows that the time required to obtain a void-free composite with press moulding of hybrid textiles is significantly larger than previously thought. Within industrial applications, the model presented in this study can be used to predict the consolidation time required to obtain acceptable porosity content rather than a void-free composite, in order to keep cycle times within reasonable bounds.

The present model can be very well implemented for consolidation processes in which the temperature is not constant, such as stamp process or for press moulding with variable temperature. In that case,

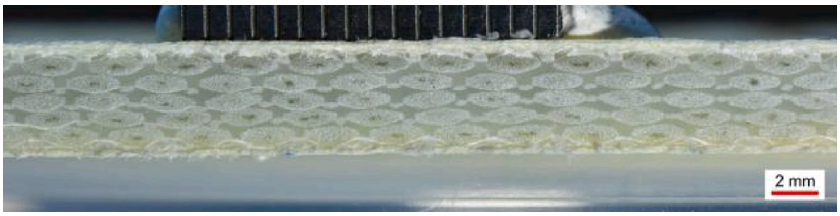


**Fig. 18.** Cross section Picture of the plate with HDPE consolidated at 6.92 MPa for 60 min. While some tows are completely impregnated, dry areas characterized by a darker shade are visible in other tows.

the dependence of viscosity and solubility on temperature needs to be modelled, respectively with an Arrhenius type function [56,57] and with the function proposed by Sato et al. [50] for instance. This implies that the consolidation model may need coupling with a thermal simulation, should the temperature through the composite not be homogeneous.

Further aspects that should be investigated in future studies include the influence of statistical effects on porosity prediction accuracy. As shown in Fig. 18, while most of the tows are completely impregnated some still present unimpregnated areas. Towards the end of consolidation it therefore becomes apparent that the consolidation process is not rigorously the same in all tows. Variation in tow dimensions, permeability or amount of entrapped air are possible explanations for these discrepancy. Possibly, understanding and taking these statistical effects into account could help to more accurately model porosity. Otherwise, press moulding under vacuum should be investigated since the time required for total impregnation can be dramatically reduced in the absence of air as shown in Fig. 13. Feasibility and economically viability studies are required to begin with since applying vacuum is technically challenging, especially at high temperatures.

## 7. Conclusion

In this article, we propose and experimentally validate an analytical model for the consolidation of hybrid textiles in which air entrapment and dissolution is considered. Direct tow permeability measurement was carried out to validate, for the first time, the analytical model of Gebart at very high fibre volume fractions and reasonably good agreement was found.

The model was found to be able to reproduce all relevant phenomena and correctly predict the consolidation behaviour for different polymers and at a range of pressures. Entrapped air is shown to have a large influence on the consolidation behaviour and complete dissolution of the air is necessary to fully consolidate the composite, which can take significant amount of time. The model offers new and comprehensive insights about the phenomena taking place during consolidation and enables future process optimization. Some material properties including the solubility and diffusion coefficient which were not taken into account so far are found to largely influence consolidation and should be characterized in future studies.

During consolidation with two-stage press moulding, the short time where no pressure is applied on the mould as it is displaced from the hot to the cold stage is found to be sufficient to induce significant deconsolidation, which has practical consequences for the industry. We recommend using rapid variotherm press moulding instead or at least minimizing the deconsolidation time.

In future work the model will be validated with high performance hybrid textiles and the influence of statistical effects on porosity prediction assessed. The feasibility of rapid variotherm press moulding coupled with vacuum and the achievable cycle times will be investigated.

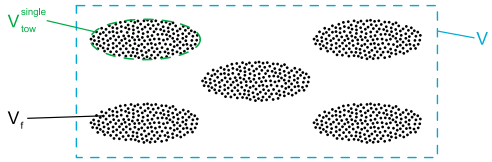


**Fig. A.19.** Schematical representation different volumes at the meso level of a stack of textile: the volume occupied by the fibres $V_f$, the volume occupied by a single tow $V_{tow}^{single}$ and the total volume $V$. The volume $V_{tow}$ is not indicated but would be the sum of the volumes occupied by the single tows $V_{tow}^{single}$.

## CRediT authorship contribution statement

**Vincent Werlen:** Conceptualization, Methodology, Data curation, Formal analysis, Investigation, Software, Validation, Visualization, Writing – original draft, Writing – review & editing. **Richard Vocke:** Writing – review & editing. **Christian Brauner:** Funding acquisition. **Clemens Dransfeld:** Supervision, Writing – original draft, Writing – review & editing. **Véronique Michaud:** Supervision, Writing – original draft, Writing – review & editing. **Christian Rytka:** Supervision, Project administration.

## Declaration of competing interest

The authors declare the following financial interests/personal relationships which may be considered as potential competing interests: Vincent Werlen reports financial support was provided by Swiss National Science Foundation. Richard Vocke reports financial support was provided by German Research Foundation.

## Data availability

Data will be made available on request.

## Acknowledgements

This work is part of the research project Consolidation of Thermoplastic hybrid yarn materials “ConThP” and is funded by the German Research Foundation [DFG Nr. 394279584] and the Swiss National Science Foundation [200021E/177210 / 1]. We kindly thank Mr. Schneeberger and Tissa Glassweberei AG for providing the textiles and for their precious support.

## Appendix. Mathematical proof

### A.1. Initial amount of entrapped air

To determine the amount of air trapped in each tow per unit depth, a stack of textile at rest as represented in Fig. A.19 with volume $V$ and depth $d$ is considered. The volume occupied by the tows, by a single tow and by the fibres are denoted respectively $V_{tow}$, $V_{tow}^{single}$ and $V_f$. The volume occupied by the tows includes everything inside the tow boundaries, meaning both the fibres and the space between them.

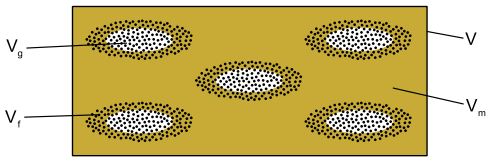


**Fig. A.20.** Schematical representation of the volume occupied by the different phases during consolidation: the volume occupied by the fibres $V_f$, the volume occupied by the air $V_g$, the volume occupied by the matrix $V_m$ and the total volume $V$.

To begin with, the fibre volume fraction at rest $v_{f,0}$ and the tow volume fractions $v_{f,tow}$ are defined as:

$$v_{f,0} = \frac{V_f}{V} \tag{A.1}$$

$$v_{f,tow} = \frac{V_f}{V_{tow}} \tag{A.2}$$

The volume occupied by the gas phase $V_g$ is directly found by subtracting the volume occupied by the fibres from the total volume. Inserting the definition of the fibre volume fraction one finds:

$$V_g = V - V_f = (1 - v_{f,0}) \cdot V \tag{A.3}$$

Assuming that the air is equally distributed, the amount of air $V_{g,tow}$ that will be pushed inside each tow is found by dividing the volume occupied by the gas phase in a given control volume with the number of tows $n_{tow}$ present in that control volume:

$$V_{g,tow} = \frac{V_g}{n_{tow}} \tag{A.4}$$

This variable is found by relating the volume occupied by the tows to the volume occupied by a single tow, which is the product of its cross-section $A_{tow}$ and its depth.

$$n_{tow} = \frac{V_{tow}}{V_{tow}^{single}} = \frac{V_{tow}}{A_{tow} \cdot d} \tag{A.5}$$

The ideal gas law is applied to determine the amount of air entrapped per tow and unit depth $n_\lambda^0$. Considering that the volume occupied by the air $V_{g,tow}$ that will be pushed in each tow is initially at atmospheric pressure $P_{atm}$ and temperature $T_0$, it is given as:

$$n_\lambda^0 = \frac{P_{atm} \cdot V_{g,tow}}{R \cdot T_0 \cdot d} \tag{A.6}$$

Finally, inserting all these together yields:

$$n_\lambda^0 = \frac{P_{atm} \cdot (1 - v_{f,0}) \cdot v_{f,tow} \cdot A_{tow}}{R \cdot T_0 \cdot v_{f,0}} \tag{A.7}$$

### *A.2. Fibre volume fraction*

The fibre volume fraction is defined as:

$$v_f = \frac{V_f}{V_f + V_m + V_g} \tag{A.8}$$

where $V_f$, $V_m$ and $V_g$ are the volume occupied respectively by the fibre, matrix and gas as represented in Fig. A.20.

The volume occupied by the fibres in a tow can be determined on the basis of their weight $M_f$ and their density through Eq. (A.9), similar considerations apply to the matrix and Eq. (A.10) relates the matrix volume to its mass $M_m$ and density.

$$V_f = \frac{M_f}{\rho_f} \tag{A.9}$$

$$V_m = \frac{V_m}{\rho_m} \tag{A.10}$$

The volume occupied by the tows $V_{tow}$ consists of the volume occupied by the fibres in the main tows $V_{f,tow}$ and the space between the fibres. The gas volume $V_g$ is equal to the space between the fibres in the volume of the unimpregnated region of the tow, which is directly related to the impregnation degree. Hence, the volume occupied by the gas can be described with Eq. (A.11) assuming that the impregnation degree is homogeneous in the composite. Putting Eqs. (A.9), (A.10), (A.11) and (A.2) into Eq. (A.8) yields Eq. (A.12):

$$V_g = V_{tow} \cdot (1 - v_{f,tow}) \cdot (1 - \xi) \tag{A.11}$$

$$v_f = \frac{\frac{M_f}{\rho_f}}{\frac{M_f}{\rho_f} + \frac{M_m}{\rho_m} + \frac{M_f}{\rho_f} \cdot \frac{(1 - v_{f,tow})}{v_{f,tow}} \cdot (1 - \xi)} \tag{A.12}$$

For $N$ layers and a cavity area $A_c$ the total fibre mass $M_f$ is found with Eq. (A.13) :

$$M_f = N \cdot A_c \cdot M_{tex}^A \tag{A.13}$$

Inserting this Equation back into Eq. (A.12) finally yields:

$$v_f = \frac{M_{tex}^A}{M_{tex}^A + \frac{M_m \rho_f}{\rho_m N A_c} + M_{tex}^A \frac{(1 - v_{f,tow})}{v_{f,tow}} (1 - \xi)} \tag{A.14}$$

## References


[1] Roux M, Eguemann N, Dransfeld C, Thiebaud F, Perreux D. Thermoplastic carbon fibre-reinforced polymer recycling with electrodynamical fragmentation: From cradle to cradle. J Thermoplast Compos Mater 2017;30(3).

[2] Witik RA, Payet J, Michaud V, Ludwig C, Månson J-aE. Assessing the life cycle costs and environmental performance of lightweight materials in automobile applications. Composites A 2011;42(11).

[3] Studer J, Dransfeld C, Cano JC, Keller A, Wink M, Masania K, Fiedler B. Effect of fabric architecture, compaction and permeability on through thickness thermoplastic melt impregnation. Composites A 2019;122.

[4] Werlen V, Rytka C, Wegmann S, Philipp H, Khalaf Y, Michaud V, Brauner C, Dransfeld C. Novel tooling for direct melt impregnation of textile with vario-thermal injection moulding: methodology and proof of concept. J Compos Mater 2022.

[5] Schneeberger C, Wong JC, Ermanni P. Hybrid bicomponent fibres for thermoplastic composite preforms. Composites A 2017;103:69–73.

[6] Gomez C, Salvatori D, Caglar B, Trigueira R, Orange G, Michaud V. Resin transfer molding of High-Fluidity Polyamide-6 with modified Glass-Fabric preforms. Composites A 2021;147.

[7] Bernet N, Wakeman MD, Bourban PE, Manson J-AE. An integrated cost and consolidation model for commingled yarn based composites. Composites A 2002;33:495–506.

[8] Wolfrath J, Michaud V, Manson J-AE. Deconsolidation in glass mat thermoplastics: Influence of the initial fibre/matrix configuration. Compos Sci Technol 2005;65:1601–8.

[9] Reynolds N, Awang-Ngah S, Williams G, Hughes DJ. Direct processing of structural thermoplastic composites using rapid isothermal stamp forming. Appl Compos Mater 2020;27(1–2):107–15.

[10] Werlen V, Vocke R, Schwanemann P, Michaud V, Brauner C, Dransfeld C, Rytka C. Consolidation of hybrid textiles for aerospace applications. In: 20th European conference on composite materials ECCM20. Lausanne, Switzerland; 2022.

[11] Saenz-castillo D, Martín MI, Calvo S, Rodriguez-lence F, Güemes A. Effect of processing parameters and void content on mechanical properties and NDI of thermoplastic composites. Composites A 2019;121(March):308–20.

[12] Dong C. Effects of process-induced voids on the properties of fibre reinforced composites. J Mater Sci Technol 2016;32(7).

[13] Gebart B. Permeability of unidirectional reinforcements for RTM. J Compos Mater 1992;26(8):1100–33.

[14] Darcy H. Les fontaines publiques de la ville de dijon. Paris: Dalmont; 1856.

[15] Jespersen ST, Wakeman MD, Michaud V, Cramer D, Manson J-AE. Film stacking impregnation model for a novel net shape thermoplastic composite preforming process. Compos Sci Technol 2008;68:1822–30.

[16] Zarandi MAF, Arroyo S, Pillai KM. Longitudinal and transverse flows in fiber tows: Evaluation of theoretical permeability models through numerical predictions and experimental measurements. Composites A 2019;119(November 2018):73–87.

[17] Godbole MG, Purandare R, Harshe R, Hood A, Gururaja S, Joshi M, Advani S. Influence of filament distribution on transverse tow permeability: Model predictions and experimental validation. Composites A 2019;118(June 2018):150–61.

[18] Gutowski TG, Cai Z, Bauer S, Boucher D, Kingery J, Wineman S. Consolidation experiments for laminate composites. J Compos Mater 1987;21:650–69.

[19] Jackson GW, James DF. The permeability of fibrous porous media. Can J Chem Eng 1986;64(3):364–74.
[20] Ali MA, Umer R, Khan KA, Bickerton S, Cantwell WJ. Non-destructive evaluation of through-thickness permeability in 3D woven fabrics for composite fan blade applications. Aerosp Sci Technol 2018;82–83:520–33.
[21] Endruweit A, Gommer F, Long AC. Stochastic analysis of fibre volume fraction and permeability in fibre bundles with random filament arrangement. Composites A 2013;49:109–18.
[22] Bernet N, Michaud V, Bourban PE, Manson J-AE. An impregnation model for the consolidation of thermoplastic composites made from commingled yarns. J Compos Mater 1999;33(8):751–72.
[23] Phillips R, Akyüz DA, Manson J-AE. Prediction of the consolidation of woven fibre-reinforced thermoplastic composites. Part I. Isothermal case. Composites A 1998;395–402.
[24] Rozant O, Michaud V, Bourban PE, Manson J-AE. A model for the consolidation of warp-knitted reinforced laminates. Polym Compos 2001;22(3).
[25] Michaud V, Manson J-AE. Impregnation of compressible fiber mats with a thermoplastic resin. part I: Theory. J Compos Mater 2001;35(13).
[26] Michaud V, Törnqvist R, Manson J-AE. Impregnation of compressible fiber mats with a thermoplastic resin. part II: Experiments. J Compos Mater 2001;35(13).
[27] Michaud V, Mortensen A. Infiltration processing of fibre reinforced composites: governing phenomena. Composites A 2001;32:981–96.
[28] Michaud V, Sommer JL, Mortensen A. Infiltration of fibrous preforms by a pure metal: Part V. Influence of preform compressibility. Metall Mater Trans A: Phys Metall Mater Sci 1999;30(2):471–82.
[29] Sommer JL, Mortensen A. Forced unidirectional infiltration of deformable porous media. J Fluid Mech 1996;311:193–217.
[30] Klinkmüller V, Um MK, Steffens M, Friedrich K, Kim BS. A new model for impregnation mechanisms in different GF/PP commingled yarns. Appl Compos Mater 1995;1:351–71.
[31] Grouve WJ, Akkerman R. Consolidation process model for film stacking glass/PPS laminates. Plast Rubber Compos 2010;39(3–5):208–15.
[32] Kobayashi S, Tsukada T, Morimoto T. Resin impregnation behavior in carbon fiber reinforced polyamide 6 composite: Effects of yarn thickness, fabric lamination and sizing agent. Composites A 2017;101:283–9.
[33] Van West BP, Pipes RB, Advani SG. The consolidation of commingled thermoplastic fabrics. Polym Compos 1991;12:417–27.
[34] Kobayashi S, Morimoto T. Experimental and numerical characterization of resin impregnation behavior in textile composites fabricated with micro-braiding technique. Mech Eng J 2014;1(4):SMM0031.
[35] Crank J. The mathematics of diffusion, Vol. 79. 2nd ed.. Oxford: Clarendron Press; 1975.
[36] Crank J. Diffusion in polymers. Academic Press; 1968.
[37] Zingraff L, Michaud V, Bourban PE, Månson JA. Resin transfer moulding of anionically polymerised polyamide 12. Composites A 2005;36(12).
[38] Fick A. Ueber diffusion. Ann Phys 1855;170(1).
[39] Wood JR, Bader MG. Void control for polymer-matrix composites (1): Theoretical and experimental methods for determining the growth and collapse of gas bubbles. Compos Manuf 1994;5(3):139–47.
[40] Epstein PS, Plesset MS. On the stability of gas bubbles in liquid-gas solutions. J Chem Phys 1950;18(11):1505–9.
[41] Zhang D, Heider D, Gillespie JW. Void reduction of high-performance thermoplastic composites via oven vacuum bag processing. J Compos Mater 2017;51(30):4219–30.
[42] Hou M, Ye L, Lee HJ, Mai YW. Manufacture of a carbon-fabric-reinforced polyetherimide (CF/PEI) composite material. Compos Sci Technol 1998;58(2):181–90.
[43] Lundström TS. Measurement of void collapse during resin transfer moulding. Composites A 1997;28(3):201–14.
[44] Szmyt W, Guerra C, Utke I. Diffusion of dilute gas in arrays of randomly distributed, vertically aligned, high-aspect-ratio cylinders. Beilstein J Nanotechnol 2017;8(1):64–73.
[45] Szmyt W, Dransfeld C, Utke I, Guerra-nu C. Solving the inverse knudsen problem : Gas diffusion in random fibrous media. J Membr Sci 2021;620(April 2020).
[46] Transvalidou F, Sotirchos SV. Effective diffusion coefficients in square arrays of filament bundles. AIChE J 1996;42(9):2426–38.
[47] Werlen V, Rytka C, Michaud V. A numerical approach to characterize the viscoelastic behaviour of fibre beds and to evaluate the influence of strain deviations on viscoelastic parameter extraction. Composites A 2021;143(October 2020):106315.
[48] Robitaille F, Gauvin R. Compaction of textile reinforcements for composites manufacturing. I: Review of experimental results. Polym Compos 1998;19(2):198–216.
[49] Danzi M, Schneeberger C, Ermanni P. A model for the time-dependent compaction response of woven fiber textiles. Composites A 2018;105:180–8.
[50] Sato Y, Fujiwara K, Takikawa T, Sumarno, Takishima S, Masuoka H. Solubilities and diffusion coefficients of carbon dioxide and nitrogen in polypropylene, high-density polyethylene, and polystyrene under high pressures and temperatures. Fluid Phase Equilib 1999;162(1–2):261–76.
[51] Wolfrath J, Michaud V, Manson J-AE. Deconsolidation in glass mat thermoplastic composites: Analysis of the mechanisms. Composites A 2005;36:1608–16.
[52] May D, Aktas A, Advani SG, Berg DC, Endruweit A, Fauster E, Lomov SV, Long A, Mitschang P, Abaimov S, Abliz D, Akhatov I, Ali MA, Allen TD, Bickerton S, Bodaghi M, Caglar B, Caglar H, Chiminelli A, Correia N, Cosson B, Danzi M, Dittmann J, Ermanni P, Francucci G, George A, Grishaev V, Hancioglu M, Kabachi MA, Kind K, Deléglise-Lagardère M, Laspalas M, Lebedev OV, Lizaranzu M, Liotier PJ, Middendorf P, Morán J, Park CH, Pipes RB, Pucci MF, Raynal J, Rodriguez ES, Schledjewski R, Schubnel R, Sharp N, Sims G, Sozer EM, Sousa P, Thomas J, Umer R, Wijaya W, Willenbacher B, Yong A, Zaremba S, Ziegmann G. In-plane permeability characterization of engineering textiles based on radial flow experiments: A benchmark exercise. Composites A 2019;121(October 2018):100–14.
[53] Sato Y, Yurugi M, Fujiwara K, Takishima S, Masuoka H. Solubilities of carbon dioxide and nitrogen in polystyrene under high temperature and pressure. Fluid Phase Equilib 1996;125:129–38.
[54] Gomarasca S, Peeters DMJ, Atli-veltin B, Dransfeld C. Characterising microstructural organisation in unidirectional composites. Compos Sci Technol 2021;215(September).
[55] Harper CA. In: Harper CA, editor. Handbook of plastic processes. New Jersey: John Wiley & Sons; 2006.
[56] Arrhenius S. Über die reaktionsgeschwindigkeit bei der inversion von rohrzucker durch säuren. Z Phys Chem 1889;4U(1):226–48.
[57] Logan SR. The origin and status of the Arrhenius Equation. J Chem Educ 1982;59(4).